J. Phys. B: At. Mol. Opt. Phys. 28 (1995) 4811–4822. Printed in the UK

Electron-impact ionization of Ar^{9+}

K Laghdas†, R H G Reid‡, C J Joachain† and P G Burke‡

† Physique Théorique, Faculté des Sciences, Université Libre de Bruxelles, Bruselles, Belgium
‡ The Department of Applied Mathematics and Theoretical Physics, The Queen's University of Belfast, Belfast BT7 1NN, UK

Received 30 May 1995, in final form 30 August 1995

Abstract. We have calculated total and single differential cross sections for electron-impact ionization of Ar^{9+} in its ground $(1s^2 2s^2 2p^5)\,^2P^o$ state by using a method that combines the distorted-wave Born approximation and the R-matrix theory. The incident and the scattered electrons are described by distorted waves, while the wavefunctions of the initial ground state of the Ar^{9+} ion and its final continuum state $(Ar^{10+} + e^-)$ are calculated by using the R-matrix approach. This allows us to take into account the excitation–autoionization process. Five states of the final Ar^{10+} ion, namely $1s^2 2s^2 2p^4\,^3P$, ^1D, ^1S and $1s^2 2s 2p^5\,^3P^o$, $^1P^o$, have been included in our calculation. Up to the 2^4-pole components of the interaction with the ionizing electron were included, exciting ten distinct Ar^{9+} continuum symmetries. The single differential cross sections exhibit considerable structure due to autoionizing resonances. Total cross sections for production of Ar^{10+} in each of the five states are presented for impact energies from the threshold energy at 17.6 to 100 au. Our theoretical values for the total cross section are in fair agreement with the experimental results.

1. Introduction

The electron-impact ionization of an ion

$$e^- + X^{q+} \longrightarrow e^- + X^{(q+1)+} + e^- \tag{1}$$

is a fundamental process in plasmas, whether laboratory (cf Mark 1992) or astrophysical (cf Shull 1993). In the study of this process, it has long been recognized (Goldberg *et al* 1965) that it is insufficient to consider only the direct ionization process, in which the incident electron brings an electron in the target ion X^{q+} from a bound orbital to a continuum state, with the other electrons of X^{q+} being spectators. Rather, it is necessary to consider also indirect processes, in which the other electrons play an active part. The ion X^{q+} can first be excited to a doubly excited quasibound state, which then autoionizes. This is the excitation–autoionization process, which can be further refined by improving the treatment of the excitation mechanism. The role of indirect processes in electron-impact ionization of positive ions has recently been reviewed by Moores and Reed (1994).

In the present work, we have used the R-matrix method of Bartschat and Burke (1987) to calculate total and single differential cross sections for electron-impact ionization. In this method, the final continuum states of X^{q+}, which are comprised asymptotically of the final ion $X^{(q+1)+}$ plus the ejected electron, are described accurately by the R-matrix method. This precise treatment of the final continuum states of X^{q+} ensures that the autoionizing levels of the target ion are included, which means that the excitation–autoionization process is included as an integral coherent part of the collisional ionization process. The initial

0953-4075/95/224811+12$19.50

bound state of X^{q+} is also calculated by the R-matrix method and is thus consistent with the final continuum states. This is a significant merit of this method. Less satisfactorily, the ionizing electron is described by the distorted-wave Born approximation, and exchange between the ionizing electron and the electrons of the target, including the ejected electron, is neglected, except for the use of the 'half-range' of ejected-electron energies. This treatment of the ionizing electron reduces the accuracy of the method when the energy of the incident electron is low or when the energies of the outgoing electrons are both low, although the errors thus incurred are smaller for highly ionized species, as in the present case. The computational details of the method and the associated computer code have been described by Bartschat (1993).

This formulation by Bartschat and Burke is similar to that used by Jakubowicz and Moores (1981) except that in the latter the inner-region solution is obtained by solving integro-differential equations for each continuum energy, which makes it very much less efficient than the R-matrix method with its energy-independent inner-region solution.

An alternative way to allow for indirect ionization is to regard it as a distinct process from direct ionization. The cross section for electron-impact excitation of the autoionizing states of X^{q+} is calculated, assuming that the autoionizing states are discrete states lying in the continuum with zero decay width. This excitation cross section, possibly reduced by a factor to allow for the branching between autoionization and radiative decay, is then added to the cross section for direct ionization. This method has been reviewed by Henry and Kingston (1988), with more recent examples given by Gorczyca *et al* (1994) and Tayal (1994). An advantage of this approach is that a more elaborate treatment of the excitation process can be used, so that features such as compound states of the $(e^- + X^{q+})$ system can be included, and thus the resonance-excitation mechanisms (REDA, READI, ...) may be incorporated. Also, electron exchange can be included, both in the $(e^- + X^{q+})$ excitation calculation and in the direct ionization calculation (cf Younger 1981). However, the quantum coherence between the direct and indirect processes is lost, as are the details of the interaction between the residual ion $X^{(q+1)+}$ and the ejected electron—it is worth recalling that most of the ionization cross section comes from slow ejected electrons. Further, only a few of the lowest members of the Rydberg series of resonances can be included, whereas our present approach includes the effect of the complete Rydberg series of resonances, as discussed in section 4.1.

The system for which we have performed calculations is Ar^{9+} in its ground $1s^22s^22p^5\ ^2P^o$ state. This provides a useful test of the method, firstly because the initial state is not an S-state (so that there may be several coupling paths to each final symmetry), and secondly because the $1s^22s^22p^4$ and $1s^22s2p^5$ configurations of the final Ar^{10+} ion give rise to a reasonably elaborate set of autoionizing states of Ar^{9+}. Also, experimental data are available for this system (Rachafi 1988). Previous applications of the Bartchat–Burke formulation have been to neutral species (Bartschat and Burke 1988, Bartschat *et al* 1990, Reid *et al* 1992, Raeker *et al* 1994). For the present application to a highly charged ion, the published code (Bartschat 1993) was modified by introducing the outer-region-solution method described by Seaton (1985).

In the next section we present a broad general outline of the theory, with no more detail than is necessary to introduce the basic quantities and parameters of the calculation. More details can be found in the paper of Bartschat and Burke (1987) and in papers cited therein. In section 3 the details of the specific calculation for Ar^{9+} are given. The results for single differential cross sections and total cross sections are presented, and compared with experiment, in section 4.

2. Theory

Figure 1 shows the ionization process (1) when resolved into partial waves. The state label a of $X^{(q+1)+}$ and the symmetry label G of X^{q+} exclude the magnetic quantum numbers, which are not shown; nor is the principal quantum number of the initial bound state of X^{q+}. The ionizing electron e_0^- has incident energy E_0. The electrostatic interaction between e_0^- and the $N+1$ electrons of X^{q+} causes e_0^- to lose energy $\Delta E \equiv E_0 - E_1$ and excites X^{q+} from the initial state G_0 (with energy $\mathcal{E}_0$) to a continuum state $Ga\ell_2$ (with energy $\mathcal{E} = \mathcal{E}_0 + \Delta E$). This continuum state represents scattering of the ℓ_2th partial wave of the ejected electron e_{N+1}^- by the final-ion $X_a^{(q+1)+}$, with incoming scattered waves. The energy of e_{N+1}^- is $E_2 = \Delta E - I_a$, where I_a is the energy of $X_a^{(q+1)+}$ relative to $X_{G_0}^{q+}$, i.e. I_a is the threshold energy loss for production of $X_a^{(q+1)+}$. The ionic energies $\mathcal{E}_0$ and $\{I_a\}$ being fixed, the collision is characterized by E_0 and ΔE.

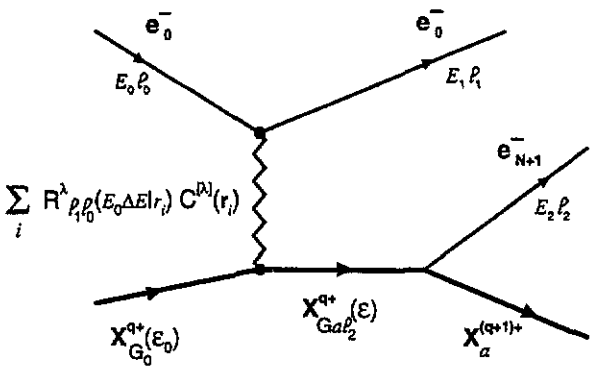

Figure 1. Model of the process $e_0^- + X_{G_0}^{q+} \longrightarrow e_0^- + X_a^{(q+1)+} + e_{N+1}^-$.

With e_0^- described by the distorted-wave Born approximation, and with all exchange effects involving e_0^- neglected, the 2^λ-pole component of the interaction, when overlapped between the ℓ_0th and the ℓ_1th partial waves of e_0^-, gives the one-electron operator $\sum_{i=1}^{N+1} R^\lambda_{\ell_1\ell_0}(E_0\Delta E|r_i)C^{[\lambda]}(\hat{\boldsymbol{r}}_i)$. This operator provides the coupling between the initial bound state Ψ^{G_0} and the final continuum state $\psi^{(-)G}_{a\ell_2\Delta E}$.

The most elementary quantity we calculate in the present work is the single differential cross section for producing $X_a^{(q+1)+}$ via continuum symmetry G:

$$\frac{\mathrm{d}\sigma}{\mathrm{d}\Delta E}(Ga\Delta E|G_0E_0) = \frac{16}{E_0\varpi_{G_0}} \sum_{\substack{\ell_0\ell_1 \\ \lambda\ell_2}} \left| \left\langle \psi^{(-)G}_{a\ell_2\Delta E} \middle\| \sum_{i=1}^{N+1} R^\lambda_{\ell_1\ell_0}(E_0\Delta E|r_i)C^{[\lambda]}(\hat{\boldsymbol{r}}_i) \middle\| \Psi^{G_0} \right\rangle \right|^2 . \quad (2)$$

If $G \equiv \gamma J$, then the weight $\varpi_{G_0} = 2J_0 + 1$, while if $G \equiv \alpha SL$ then effectively $\varpi_{G_0} = 2L_0 + 1$ and a factor δ_{SS_0} appears. The continuum radial functions in (2) are normalized so that asymptotically their incident parts are $k^{-1/2}$ times a sine function.

The total cross section for producing $X_a^{(q+1)+}$ via continuum symmetry G is given, using the half-range approximation, by

$$\sigma(Ga|G_0E_0) = \int_{I_a}^{\frac{E_0+I_a}{2}} \frac{\mathrm{d}\sigma}{\mathrm{d}\Delta E}(Ga\Delta E|G_0E_0)\,\mathrm{d}\Delta E. \quad (3)$$

The physically significant total cross sections are obtained by summing over G. However, the detailed information on autoionizing resonances is contained in the single differential cross section for a specific G.

An important shortcoming of using only the non-exchange single differential cross section in the half-range approximation (3) has been noted by Moores and Reed (1989). According to (3), an autoionizing resonance, the energy of which relative to the initial state is $\mathcal{E}_r$, contributes to $\sigma(Ga|G_0E_0)$ only for $E_0 \geqslant 2\mathcal{E}_r - I_a$, rather than for the correct threshold $E_0 \geqslant \mathcal{E}_r$. However, in the present case we shall see that this shift in the threshold by $\mathcal{E}_r - I_a$ does not cause appreciable errors in our results.

3. Computational details

We have considered ionization of fluorine-like Ar^{10+} in its ground state, and have included five states of the final Ar^{10+} ion:

$$e^- + Ar^{9+}\left(2s^22p^5\right)\,{}^2P^o \longrightarrow \begin{cases} 2e^- + Ar^{10+}\left(2s^22p^4\right)\,{}^3P & (I_1 = 17.595\,947 \text{ au}) \\ 2e^- + Ar^{10+}\left(2s^22p^4\right)\,{}^1D & (I_2 = 17.892\,384 \text{ au}) \\ 2e^- + Ar^{10+}\left(2s^22p^4\right)\,{}^1S & (I_3 = 18.241\,441 \text{ au}) \\ 2e^- + Ar^{10+}\left(2s2p^5\right)\,{}^3P^o & (I_4 = 20.006\,493 \text{ au}) \\ 2e^- + Ar^{10+}\left(2s2p^5\right)\,{}^1P^o & (I_5 = 20.893\,054 \text{ au}). \end{cases} \tag{4}$$

Each Ar^{10+} state is described by a single configuration, except that ^1S is an admixture with $1s^22p^6$. The bound 1s, 2s and 2p radial orbitals from which the wavefunctions are constructed were obtained from those given by Clementi and Roetti (1974) for $1s^22s^22p^4\,{}^3P$, reoptimized to the sum of the energies of the ^3P, ^1D and ^1S states using the CIV3 code (Hibbert 1975). Empirical ionization and excitation energies were imposed. These were obtained by taking the weighted term averages of the data given by Bashkin and Stoner (1981). The energies of the Ar^{10+} states relative to the ground state of Ar^{9+} states (the quantities I_a) are shown in (4).

Regarding the interaction between the ionizing electron and the electrons of Ar^{9+}, the 2^λ-pole components with $\lambda = 0, \ldots, 4$ were included in our calculation (except at the highest impact energies—see below). This implies that the $^2P^o$ initial state can be excited to ten final continuum symmetries. Table 1 shows these final symmetries (column 1) and the λ-values that excite them (column 2). Table 1 also shows the orbital angular momentum ℓ_2 of the electron which, when coupled to an Ar^{10+} state, will produce the final symmetry. The number of coupled channels (i.e. distinct $a\ell_2$ values) for each symmetry can be read off. The maximum number of channels is nine. The maximum ℓ_2-value that occurs is seven.

Based on the ranges of the radial orbitals, the R-matrix radius was taken to be 1.984 a_0. Ten continuum orbitals were constructed for each ℓ_2, for $\ell_2 = 0, \ldots, 7$. The wavefunction for the initial bound $1s^22s^22p^5\,{}^2P^o$ state of Ar^{9+}, constructed by the R-matrix code, is thus comprised of $10 \times 8 + 1 = 81$ configurations including the $1s^22s^22p^5\,{}^2P^o\ L^2$ configuration. The eigenenergy obtained is $-490.523\,62$ au, which compares favourably with the value of $-490.479\,41$ au given by Clementi and Roetti (1974), and is indicative of the quality of the wavefunction. The consistency between this bound wavefunction and the continuum wavefunctions is an important feature of the calculation. In particular, the orthogonality of the bound wavefunction to the continuum wavefunctions is generally guaranteed, since this

Table 1. Couplings and resonances for each final continuum symmetry of Ar^{9+}. The values of λ are those for which there is electric 2^λ-pole coupling from the initial Ar^{9+} $(2s^2 2p^5)\,^2P^o$ state. For each Ar^{10+} core, ℓ_2 is a possible value of the added electron, while n^*_{min} is the lowest effective principal quantum number for which an autoionizing resonance has been identified in our results.

		Ar^{10+} cores								
		$^3P^e$	$^1D^e$		$^1S^e$		$^3P^o$		$^1P^o$	
Ar^{9+} symmetry	λ	ℓ_2	ℓ_2	n^*_{min}	ℓ_2	n^*_{min}	ℓ_2	n^*_{min}	ℓ_2	n^*_{min}
$^2S^e$	1	—	d	—	s	12.71	p	5 816	p	4.772
$^2P^o$	0, 2	p	p	13.766	p	8.839	s	4.657	s	4.642
			f	13.884			d	4.978	d	3.928
$^2P^e$	1, 3	s	d	13.928	—		p	4.774	p	4.770
		d								
$^2D^o$	2	p	p	13.766	—		d	4.945	d	3.932
		f	f	13.942						
$^2D^e$	1, 3	d	s	13.639						
			d	13.931	d	9.008	p	4.772	p	4.762
			g	—			f	4.994	f	3.994
$^2F^o$	2, 4	f	p	13.662						
			f	13.818	f	10.083	d	4.937	d	3.919
			h	14.006			g	4.998	g	4.998
$^2F^e$	3	d	d	13.928	—		f	5.002	f	3 998
		g	g	12.999						
$^2G^o$	4	f	f	13.000	—		g	5.004	g	5.004
		h	h	—						
$^2G^e$	3	g	d	13.911						
			g	12 999	g	—	f	4.994	f	4.993
			i	—			h	—	h	5.999
$^2H^o$	4	h	f	12.987						
			h	—	h	12.05	g	4.999	g	4.999
			j	—			i	—	i	—

property is true of the respective R-matrix bases. However, an unfortunate consequence of using the empirical energies of Ar^{10+} for the continuum $^2P^o$ state but not for the bound $^2P^o$ state is that these states are not exactly orthogonal. Hence, in the $\lambda = 0$ component of the interaction, the expression $1/\max(r_i, r_0) - 1/r_0$ was used, where r_0 is the radial coordinate of the ionizing electron.

The distorted waves for the ionizing electron, both incoming at energy E_0 and outgoing at energy E_1, were calculated in the static potential of Ar^{9+} obtained with the wavefunction given by Clementi and Roetti (1974). The number of partial waves used ranged from about 20 when $E_0 \simeq 20$ au to 100 when $E_0 = 100$ au (in practice, undistorted waves were used when the potential phase-shifts had fallen below 10^{-5}). The number of radial operators $\{R^\lambda_{\ell_1 \ell_0}\}$ increases strongly with the number of partial waves. At the two highest E_0-values considered (70 and 100 au) the required number of partial waves had increased to the

extent that it was necessary to reduce the maximum interaction multipole from 2^4-pole to quadrupole. Reducing to $\lambda \leqslant 2$ not only greatly reduces the number of radial operators, but also reduces the number of final symmetries to six and the maximum required ℓ_2-value to five (cf table 1).

The usual procedure (Bartschat 1993) is to calculate the single differential cross sections at the full mesh of ΔE values (about 10000 values) as far as the final continuum state is concerned but with the value of ΔE in the radial operators $\left\{R^{\lambda}_{\ell_1\ell_0}(E_0\Delta E)\right\}$ held fixed at a 'key' value, and to repeat the calculation for several different key ΔE values. Subsequently, for each ΔE, the cross section with the correct radial operators is found by interpolating among the results at the key values. We followed this interpolation procedure for ΔE above the $Ar^{10+}(^1P^o)$ threshold, taking three equally spaced key values between that threshold and the maximum required ΔE. However, in the narrow region between the ^3P and the ^1D thresholds only one key value of ΔE was used, without interpolation. The same was done between the ^1D and the ^1S thresholds and between the $^3P^o$ and the $^1P^o$ thresholds. Between the ^1S and the $^3P^o$ thresholds, two key values and interpolation were used.

4. Results

4.1. Single differential cross sections

Figure 2 shows the single differential cross sections for an impact energy of 40 au. These cross sections are for specific final symmetries G, and have been summed over the final-ion states. Three final symmetries (namely $^2G^o$, $^2G^e$and $^2H^o$) are not shown, largely for convenience, but also because they are less significant. Also, the cross sections have not been shown above the $Ar^{10+}(^1P^o)$ threshold because they decrease uniformly in that range, without any resonant structure. However, it should be borne in mind that, when $E_0 = 40$ au, the upper limit of ΔE contributing to the total cross section is 30.45 au, so that only about one third of the ΔE range is shown in figure 2.

The relative sizes of the single differential cross sections for various symmetries show that the couplings with $\lambda \leqslant 2$ dominate. Thus, the largest cross section is for the $^2D^e$ symmetry, which is coupled to the initial state by $\lambda = 1$, while the smallest cross section shown is for the $^2F^e$ symmetry, which is coupled by $\lambda = 3$. On the other hand, too categorical a statement cannot be made: for example, the $^2S^e$ cross section (due to $\lambda = 1$) is smaller than the $^2D^o$ cross section (due to $\lambda = 2$).

Figure 3 brings together the contributions from the individual final symmetries in the region of a significant resonance structure at about 17.96 au. It shows that, although the $^2D^e$ symmetry gives the largest background, the peak in the $^2F^o$ symmetry exceeds it by nearly two orders of magnitude. The resonances are due to quasibound autoionizing states comprised of an electron bound to an excited Ar^{10+} core. The designations of the resonances were deduced by finding the Ar^{10+} core such that the effective principal quantum number n^* is given by $n^* = n - \delta$, with n an integer and the quantum defect δ virtually constant for each series. The consistency of the shapes of the resonances within a series was also taken into account. We have identified 48 distinct series of resonances, and table 1 shows the lowest n^* of each identified series. (From table 1 it can be seen that there are potentially 57 series of resonances, but those involving $\ell_2 \geqslant 5$ are too narrow to be significant.) The series which have a $^1D^e$ or a $^1S^e$ core start with comparatively high n^*-values, and since the width of a resonance is proportional to $(n^*)^{-3}$, it follows that these series exhibit only narrow resonances. For these series, the quantum defect for the lowest n^*-value (shown in

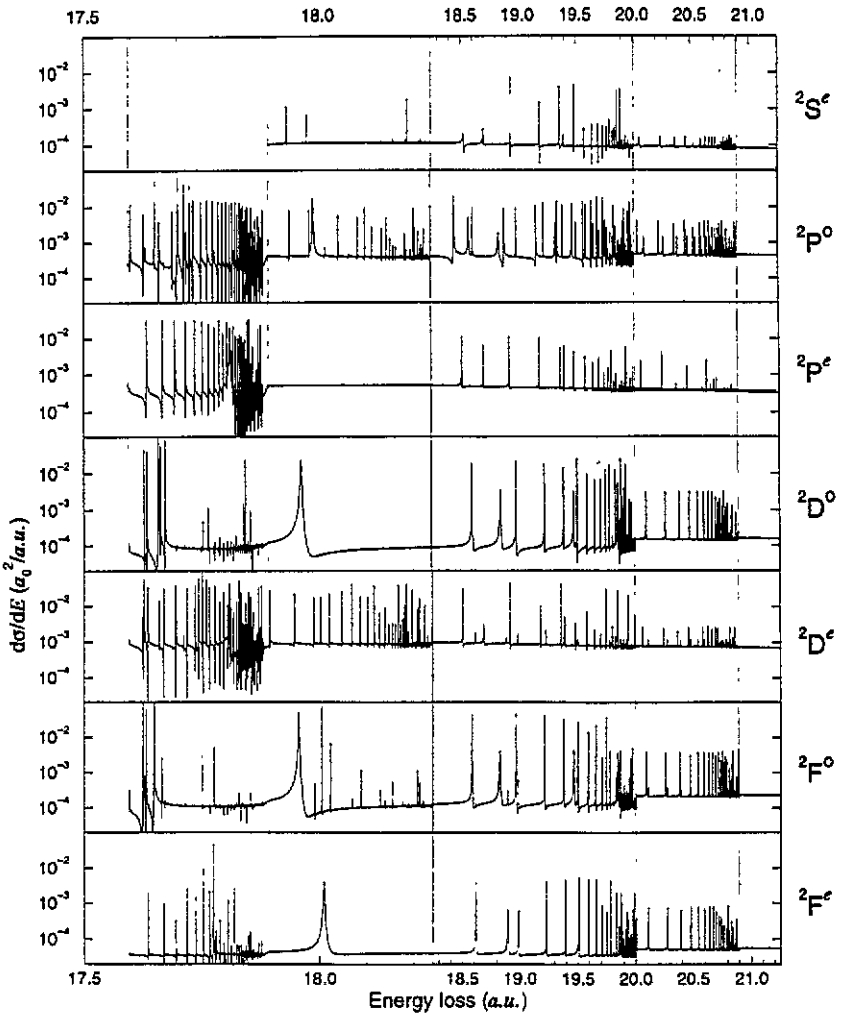

Figure 2. Contributions to the single differential cross section for ionization of Ar^{9+} by electrons with an energy of 40 au. Each contribution is from a particular continuum symmetry of Ar^{9+}, shown at the right margin, and is summed over the final states of Ar^{10+}. The vertical lines are at the thresholds for production of each final state of Ar^{10+}, namely, the $(2s^22p^4)\ ^3P$, ^1D, ^1S and $(2s2p^5)\ ^3P^o$, $^1P^o$ states, respectively (cf equation (4)). Note that the energy scale changes by a factor of four at the $(1s^22s^4)\ ^1S$ threshold.

table 1) applies to all members of the series. Resonances with low n^*-values are seen only with the $^3P^o$ and $^1P^o$ cores.

Table 2 shows the resonance energy $\mathcal{E}_r$, width Γ_r (i.e. the full width at half maximum) and effective principal quantum number n^* for some resonances with $n \leqslant 6$. As noted above, such small values of n occur only for resonances with an $Ar^{10+}\ (1s^22s2p^5)$ core. The values of $\mathcal{E}_r$ and Γ_r were obtained by fitting the single differential cross section of a particular final-continuum symmetry to a Fano profile with a linear background cross section. This analysis is possible only if the resonance is isolated, which is freqently not the case below the $^1D^e$ or $^1S^e$ thresholds. For example, the $(^1P^o\,4d)\ ^2D^o$ resonance at 17.6591 au (equivalent to $n^* \simeq 3.932$, cf table 1), is overlapped by both the $(^1D^e\,14f)\ ^2D^o$ resonance

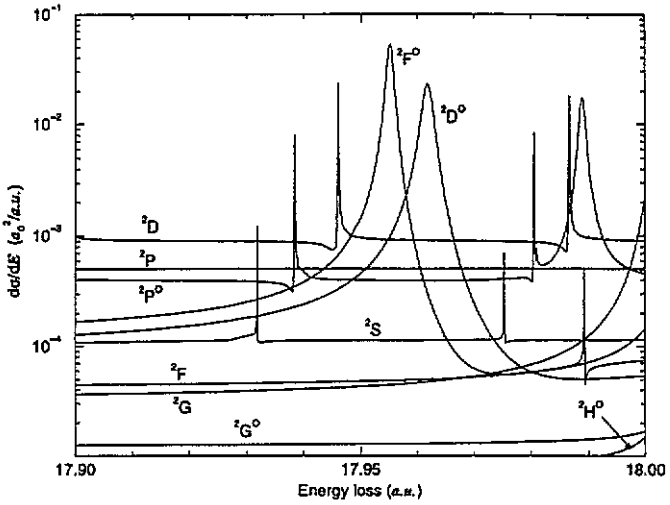

Figure 3. As in figure 2, but showing details of some prominent resonances, namely, the $2s2p^5\,(^3P^o)\,5d\,^2F^o$ resonance at 17.955 200 au, the $2s2p^5\,(^3P^o)\,5d\,^2D^o$ resonance at 17.961 847 au and the $2s2p^5\,(^3P^o)\,5d\,^2P^o$ resonance at 17.988 817 au. The other narrower resonances are $2s^22p^4\,(^1S^e)\,n\ell$ states, with $n = 13$ or 14.

at 17.6351 au and the $(^1D^e\,15p)\,^2D^o$ resonance at 17.6639 au. Similarly, the $(^1P^o\,4d)\,^2F^o$ resonance at $n^* \simeq 3.919$ (cf table 1) is overlapped by the $(^1S^e\,9f)\,^2F^o$ resonance.

It is interesting to compare the effective quantum numbers found for the autoionizing states with those for known bound states. Bashkin and Stoner (1981) list four states of Ar^{9+} with symmetries that arise in our calculation: (i) $2s2p^53s\,^2P^o$ at 12.867 au; (ii) $2s^22p^43s\,^2S^e$ at 10.963 au; (iii) $2s^22p^43s\,^2D^e$ at 10.606 au; and (iv) $2s^22p^43d\,^2P^e$ at 12.143 au. If the core in case (i) is taken to be $2s2p^5\,^3P^o$, then the experimental energy level is equivalent to $n^* = 2.646$, which is consistent with our n^*-value of 4.657 for $(^3P^o\,5s)\,^2P^o$ (cf table 1). Similarly, cases (ii)–(iv) imply $(^1S^e\,s)\,^2S^e$ with $n^* = 2.621$, $(^1D^e\,s)\,^2D^e$ with $n^* = 2.615$ and $(^1D^e\,d)\,^2P^e$ with $n^* = 2.949$, respectively, compared with our lowest resonances at n^*-values of 12.71, 13.639 and 13.928, respectively (cf table 1).

4.2. Total cross sections

The total cross sections for production of each Ar^{10+} state, obtained by integrating the single differential cross sections with respect to energy loss (cf equation 3) and summing over the final symmetries G, are shown in table 3.

Regarding the relative sizes, for impact energies well above the thresholds the cross sections for final states with the same configuration are roughly in proportion to the statistical weights of the terms. Thus, the cross sections for the $2s^22p^4\,^3P$, ^1D and ^1S states, all produced by the removal of a 2p electron, are roughly in the ratio 9:5:1. Similarly, the cross sections for the $2s2p^5\,^3P^o$ and $^1P^o$ states, both produced by the removal of a 2s electron, are roughly in the ratio 9 : 3.

The total cross sections, summed over the final Ar^{10+} states, shown in column 2 of table 3, are also plotted in figure 4, where they are compared with the experimental results of Rachafi (1988), obtained using the experimental technique described by Brouillard and Defrance (1983). The main feature of that comparison is that, in the region of the maximum cross section, our calculated results exceed the experimental results by about 20%. This is a

Table 2. Details of autoionizing states of Ar^{9+} with configuration $1s^22s2p^5\,(^3P^o)\,n\ell$ or $1s^22s2p^5\,(^1P^o)\,n\ell$, for $n \leqslant 6$. The energies are relative to the ground state $Ar^{9+}\ (2s^22p^5)\ ^2P^o$. The thresholds for production of $Ar^{10+}\,(1s^22s2p^5)\ ^3P^o$ and $Ar^{10+}\,(1s^22s2p^5)\ ^1P^o$ are 20.006 493 and 20.893 054 au, respectively. These values have been used to calculate the effective principal quantum number n^*.

Ar^{9+} symmetry	Energy $\mathcal{E}_r$ (au)	Width Γ_r (10^{-3} au)	Ar^{9+} term ($1s^22s2p^5\ldots$)	n^*
$^2S^e$	18.528 299	3.053	$(^3P^o)\,6p\,^2S^e$	5.8159
	18.697 141	4.227	$(^1P^o)\,5p\,^2S^e$	4.7717
	19.394 820	2.091	$(^1P^o)\,6p\,^2S^e$	5.7769
$^2p^o$	17.652 205	0.044	$(^1P^o)\,4d\,^2P^o$	3.9279
	17.988 817	1.267	$(^3P^o)\,5d\,^2P^o$	4.9781
	18.444 283	1.534	$(^3P^o)\,6s\,^2P^o$	5.6574
	18.572 445	4.144	$(^1P^o)\,5s\,^2P^o$	4.6418
	18.605 181	0.594	$(^3P^o)\,6d\,^2P^o$	5.9733
	18.832 641	7.445	$(^1P^o)\,5d\,^2P^o$	4.9262
$^2p^e$	18.508 013	0.891	$(^3P^o)\,6p\,^2P^e$	5.7764
	18.695 212	0.465	$(^1P^o)\,5p\,^2P^e$	4.7697
	19.392 067	0.230	$(^1P^o)\,6p\,^2P^e$	5.7716
$^2D^o$	17.961 847	2.179	$(^3P^o)\,5d\,^2D^o$	4.9451
	18.590 855	1.266	$(^3P^o)\,6d\,^2D^o$	5.9430
	18.837 704	4.284	$(^1P^o)\,5d\,^2D^o$	4.9322
	19.471 663	2.288	$(^1P^o)\,6d\,^2D^o$	5.9310
$^2D^e$	18.001 990	0.082	$(^3P^o)\,5f\,^2D^e$	4.9944
	18.505 627	0.292	$(^3P^o)\,6p\,^2D^e$	5.7718
	18.614 836	0.251	$(^3P^o)\,6f\,^2D^e$	5.9940
	18.688 175	2.826	$(^1P^o)\,5p\,^2D^e$	4.7620
	18.886 124	5.790	$(^1P^o)\,5f\,^2D^e$	4.9914
	19.499 600	3.172	$(^1P^o)\,6f\,^2D^e$	5.9902
$^2F^o$	17.955 200	1.362	$(^3P^o)\,5d\,^2F^o$	4.9371
	18.587 510	0.729	$(^3P^o)\,6d\,^2F^o$	5.9360
	18.826 923	4.969	$(^1P^o)\,5d\,^2F^o$	4.9193
	19.465 776	2.666	$(^1P^o)\,6d\,^2F^o$	5.9188
$^2F^e$	18.008 459	2.222	$(^3P^o)\,5f\,^2F^e$	5.0025
	18.618 269	1.204	$(^3P^o)\,6f\,^2F^e$	6.0014
	18.894 006	3.541	$(^1P^o)\,5f\,^2F^e$	5.0012
$^2G^o$	18 009 447	0.884	$(^3P^o)\,5g\,^2G^o$	5.0037
	18.619 288	0.594	$(^3P^o)\,6g\,^2G^o$	6.0036
	18.895 999	0.986	$(^1P^o)\,5g\,^2G^o$	5.0037
$^2G^e$	18.001 507	2.180	$(^3P^o)\,5f\,^2G^e$	4.9938
	18.614 333	1.552	$(^3P^o)\,6f\,^2G^e$	5.9929
	18.887 237	4.088	$(^1P^o)\,5f\,^2G^e$	4.9927
$^2H^o$	18.005 695	0.610	$(^3P^o)\,5g\,^2H^o$	4.9990
	18.617 021	0 504	$(^3P^o)\,6g\,^2H^o$	5.9987
	18.892 513	0.776	$(^1P^o)\,5g\,^2H^o$	4.9993

common feature of calculations in which the ionizing electron is described by the distorted-wave Born approximation without exchange (cf Jakubowicz and Moores 1981, Moores and Reed 1994).

It is of interest to estimate the contribution that the autoionizing resonances make to the total cross section. As an example, we consider the $(^3P^o\,5d)\,^2F^o$ resonance at 17.955 au, when the impact energy is 40 au (cf figure 3). Neglecting the interference

Table 3. Total cross sections for electron-impact ionization of Ar^{9+} with production of Ar^{10+} in various states (columns 3–7). Column 2 (Σ) is the cross section summed over the states of Ar^{10+}.

Impact energy	Cross section (a_0^2)					
(au)	Σ	$2s^22p^4\ ^3P^e$	$2s^22p^4\ ^1D^e$	$2s^22p^4\ ^1S^e$	$2s2p^5\ ^3P^o$	$2s2p^5\ ^1P^o$
17.6	6.234^{-6a}	6.234^{-6}				
17.8	5.342^{-4}	5.342^{-4}				
17.9	9.913^{-4}	9.837^{-4}	7.568^{-6}			
18.2	2.083^{-3}	1.832^{-3}	2.516^{-4}			
18.3	2.365^{-3}	2.003^{-3}	3.551^{-4}	6.857^{-6}		
20.0	6.612^{-3}	4.600^{-3}	1.744^{-3}	2.677^{-4}		
20.2	7.010^{-3}	4.780^{-3}	1.874^{-3}	2.944^{-4}	6.193^{-5}	
25.0	1.351^{-2}	7.524^{-3}	3.800^{-3}	6.789^{-4}	1.204^{-3}	3.022^{-4}
30.0	1.749^{-2}	9.389^{-3}	4.774^{-3}	8.764^{-4}	1.915^{-3}	5.357^{-4}
35.0	1.975^{-2}	1.042^{-2}	5.317^{-3}	9.834^{-4}	2.346^{-3}	6.782^{-4}
40.0	2.071^{-2}	1.073^{-2}	5.582^{-3}	1.024^{-3}	2.603^{-3}	7.644^{-4}
45.0	2.125^{-2}	1.093^{-2}	5.705^{-3}	1.047^{-3}	2.750^{-3}	8.148^{-4}
50.0	2.137^{-2}	1.094^{-2}	5.716^{-3}	1.053^{-3}	2.826^{-3}	8.425^{-4}
60.0	2.097^{-2}	1.065^{-2}	5.585^{-3}	1.032^{-3}	2.849^{-3}	8.552^{-4}
70.0	1.967^{-2}	1.005^{-2}	5.134^{-3}	9.073^{-4}	2.503^{-3}	6.095^{-4}
100.0	1.517^{-2}	7.875^{-3}	4.175^{-3}	7.700^{-4}	1.817^{-3}	5.321^{-4}

[a] x^y here stands for $x \times 10^y$.

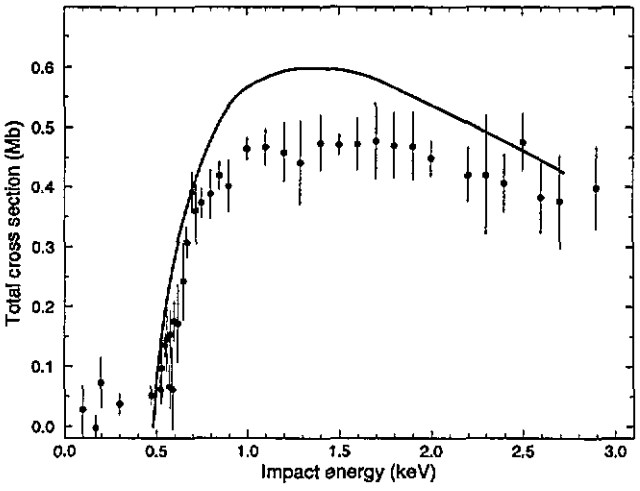

Figure 4. Total cross sections for electron-impact ionization of Ar^{9+}, summed over the final states of Ar^{10+}. The full curve is an interpolatory spline fit to our results in table 3. The points are the experimental results of Rachafi (1988).

with the background, so that the contribution to the total cross section from the resonance in the single differential cross section is $(\pi/2)\Gamma_r(d\sigma/d\Delta E)_{max}$, we estimate the contribution from the $(^3P^o\,5d)\,^2F^o$ resonance to be about $1.1 \times 10^{-4}\ a_0^2$, which is only about 0.6% of the total cross section at this value of E_0 (cf table 3). The contribution from the entire $(^3P^o\,d)\,^2F^o$ series may be estimated by assuming that $(d\sigma/d\Delta E)_{max}$ is independent of n and that $\Gamma_r \propto (n^*)^{-3}$. The ratio of the contribution for the entire series to the 5d contribution is then $(5-\delta)^3 \sum_{n=5}^{\infty}(n-\delta)^{-3} \simeq 3.0$ (since $\delta = 0.0629$). Hence this series, which is among

the most prominent (cf figure 2), contributes less than 2% to the total cross section due to the incorrect resonance thresholds arising from the use of approximation (3). Firstly, the maximum E_0 at which these errors can occur is $2I_5 - I_1 = 24.19$ au $= 0.658$ keV. Thus the errors are confined to the near-threshold region of figure 4. Secondly, for a more specific illustration let us consider the $(^3P^o\ 5d)\ ^2F^o$ resonance at 17.955 au. In the total cross section for producing $Ar^{10+}(^3P)$, the threshold for this resonance is shifted from 17.955 to 18.314 au. In this E_0-range, the total cross section increases rapidly from about $1 \times 10^{-3}\ a_0^2$ to $2 \times 10^{-3}\ a_0^2$ (cf table 3), while the contribution from the resonance (estimated as above) is about $1.9 \times 10^{-4}\ a_0^2$. Hence, mainly because the resonance contribution is less than 20% even at 17.955 au, but also because the shift in threshold is so small (9.8 eV), the effect of the threshold error is slight. Our overall conclusion is that, for ionization of Ar^{9+}, the errors due to the incorrect resonance thresholds are not appreciable. Hence, for this particular species, we did not consider it worthwhile to explore remedies (such as that proposed by Moores and Reed (1989)).

5. Summary

Our calculations of electron-impact ionization of Ar^{9+}, performed using the Bartschat–Burke R-matrix formulation to describe the initial (bound) state and the final (continuum) state of the ion, have demonstrated the capability of the method to take into account excitation–autoionization in a fully coherent way. We have presented and analysed the corresponding structure seen in the single differential cross section.

Total cross sections, for leaving Ar^{10+} in one of five states, have been presented for a wide range of impact energies. Our total cross section, summed over the final states, exceed the experimental results of Rachafi (1988) by about 20%. The contribution of autoionizing resonances to the total cross section, while not negligible, is not very significant, being of the order of a few per cent.

Acknowledgments

We gratefully acknowledge support from the UK EPSRC (grant GR/H59862), from the EC–HCM programme (contracts ERB CHRX CT 920013 and ERB CHRX CT 930350), and from the Institute Interuniversitaire des Sciences Nucléaires (Belgium). One of us (KL) thanks the Moroccan Education Ministry for a postgraduate studentship, and the Université Libre de Bruxelles for additional support.

References

Bartschat K 1993 *Comput Phys. Commun.* **17** 219
Bartschat K and Burke P G 1987 *J. Phys. B: At. Mol. Phys.* **20** 3191
—— 1988 *J. Phys. B: At. Mol. Opt. Phys.* **21** 2969
Bartschat K, Reid R H G and Burke P G 1990 *J. Phys. B: At. Mol. Opt. Phys.* **23** L721
Bashkin S and Stoner J O 1981 *Atomic Energy-Levels and Grotian Diagrams* vol 2 (Amsterdam: North-Holland) pp 250–3
Brouillard F and Defrance P 1983 *Phys. Scr.* T **3** 801
Burke P G, Fon W C and Kingston A E 1984 *J. Phys. B: At. Mol. Phys.* **17** L733
Burke P G, Kingston A E and Thompson A 1983 *J. Phys B: At. Mol. Phys.* **16** L385
Clementi E and Roetti C 1974 *At. Data Nucl. Data Tables* **14** 177

Goldberg L, Dupree A K and Allen J W 1965 *Ann. Astrophys.* **28** 589
Gorczyca T W, Pindzola M S, Griffin D C and Badnell N R 1994 *J. Phys. B: At. Mol. Opt. Phys.* **27** 2399
Griffin D C, Bottcher C and Pindzola M S 1982 *Phys. Rev.* A **25** 154
Henry R J W and Kingston A E 1988 *Adv. At. Mol. Phys.* **25** 267
Hibbert A 1975 *Comput. Phys. Commun.* **9** 141
Jakubowicz H and Moores D L 1981 *J. Phys. B: At. Mol. Phys.* **14** 3733
Mark T D 1992 *Plasma Phys. Control. Fusion* **34** 2083
Moores D L and Reed K J 1989 *Phys. Rev.* A **39** 1747
—— 1994 *Adv. At. Mol. Phys.* **34** 301
Rachafi S 1988 *PhD Thesis* Université Catholique de Louvain
Racker A, Bartschat K and Reid R H G 1994 *J. Phys. B: At. Mol. Opt. Phys.* **27** 3129
Reid R H G, Bartschat K and Burke P G 1992 *J. Phys. B: At. Mol. Opt. Phys.* **25** 3175
Seaton M J 1985 *J. Phys. B: At. Mol. Phys.* **18** 2111
Shull J M 1993 *Phys. Scr.* T **47** 165
Tayal S S 1994 *Phys. Rev.* A **49** 2561
Tayal S S and Henry R J W 1986 *Phys. Rev.* A **33** 3825
Younger S M 1981 *Phys. Rev.* A **22** 111